JOURNAL OF PROPULSION AND POWER
Vol. 18, No. 1, January–February 2002

Effects of Grain Geometry on Pulse-Triggered Combustion Instability in Rocket Motors

Mehdi Golafshani,* Mohammad Farshchi,† and Hojat Ghassemi‡
Sharif University of Technology, 11365 Tehran, Iran

Grain geometry is an important factor affecting the stability envelop of solid rocket motors. This paper presents a series of subscale tactical motor firings, clearly showing the effect of combustion chamber internal geometry on stability. Three types of grain cartridges were used in these motors: a circular perforation (CP) and two variations of a seven-pointed star. Combination of these three basic grains produced motors that have completely different internal geometries. A polyurethane-based 81% solids composite propellant was used in all tests. This marginally stable propellant has a nominal burning rate of 7.1 mm/s for the metalized formulation that contains 7% aluminum powder and 5.7 mm/s for the nonmetalized version, both at the pressure of 6.9 MPa. A pulsing technique employing gunpowder charge was developed to initiate instability, producing a pressure wave of about 10–15% of the mean operating pressure at the time of initiation. A multipulse technique was used in motors exhibiting stable behavior to ascertain the stability property. It is demonstrated that certain grain arrangements in these motors show stable behavior. In particular, repeated experimental firings clearly show that STAR-STAR (head end segment-aft end segment), CP-CP, and CP-STAR configurations lead to unstable motor behavior while the case of STAR-CP configuration, despite multipulse application, offers a great stability margin during entire motor firing.

Introduction

COMBUSTION instability is a major problem in the design, development, and operation of solid-propellant rocket motors.[1] Propellant chemical composition, internal grain configuration, and mean axial pressure variation are the key factors that can affect the stability envelop of a given motor. Expulsion of inert material such as insulation fragments can lead to a sequence of events that results in either total rocket destruction or severe pressure and thrust oscillations which can seriously damage the missile system. The physical process of combustion instability starts from a small compression wave that is created by sudden ejection of inert material through the nozzle or a localized burn-area increase as a result of the existence of random voids in the solid propellant. As this wave travels through the free volume of the motor, it will locally alter the amount of heat transferred through the combustion zone to the pyrolyzing solid propellant, which changes the local propellant burn rate. Changes in the burn rate will cause further pressure waves, and the cycle is repeated again. Full understanding of this nonlinear coupling between flow, heat transfer, and combustion has been the main goal of numerous analytical and experimental studies during the past three decades. The stability margin is governed by a balance between the sources and sinks of oscillatory energy in the combustion chamber.[2,3] Flow turning, viscosity, particulate phase, and nozzle all absorb energy from the mean flow. The primary source factor is the propellant combustion and its response to pressure and velocity coupling. In recent years vortex shedding has also been identified as an additional source of acoustic energy.[4,5] This seems to be particularly true in large segmented motors.[6,7] The role of internal grain geometry is somewhat less clear in the overall stability of motor operation.

Hart and McClure[8] and Tien[9] have reviewed analytical studies, oriented toward a basic understanding of combustion instability in solid rocket motors. Despite extensive efforts on the part of many investigators, a satisfactory theoretical understanding of all physical processes occurring in a combusting solid rocket is not yet at hand.

On the experimental side of the problem, from the earlier work of Brownlee[10] to the more recent work by Blomshield et al.[11,12] and Harris and DeChamplain[13] extensive studies and databases exist in the literature. These studies characterize the effects of propellant formulation, propellant burning rate, initial propellant temperature, motor scale, and grain configuration on combustion instability.

An interesting study carried out to characterize the effects of grain configurations on combustion instability is the work of Koreki et al.[14] They used a series of small test motors, with various grain configurations, to examine the relationship between the longitudinal mode oscillatory combustion and the motor geometry. Their tests showed that axial oscillation is closely related to a change of the port area along the motor axis. The grains used in their work were simple circular perforations (CPs) modified by gradual stepwise increase or decrease. The key conclusions reached in their work are that straight and convergent port configurations tend to suppress oscillations, whereas divergent port configurations enhance instability. Unfortunately, these results have almost gone unnoticed by motor designers and performance analysts.

In late 1994 an experimental investigation was initiated to further study the effects of common tactical motor grain geometries on pulse-triggered combustion instability. The impetus for this study was the selection of an optimum grain, in terms of combustion stability, which would be used to design a full-scale tactical rocket motor utilizing metalized solid propellant. This motor was scaled down, and a two-segment modular rocket motor was designed that could accommodate different propellant grain cartridges. Solid fuel cartridges were loaded with a baseline propellant containing 81%-solids ammonium perchlorate (AP)/polyurethane (PU)/Al propellant. Both metalized and nonmetalized variations of this baseline propellant were used in this study. To excite a motor and trigger unstable behavior, a pyrotechnic pulser was also designed. The pressure measurement instrumentation system included a Kistler 601A high-frequency piezoelectric-type pressure transducer, Shape Instruments low-frequency strain-gauge-type pressure transducers, a 16-bit multichannel and parallel A/D data acquisition system with

Received 5 July 1999; revision received 18 August 2000; accepted for publication 12 July 2001.

*Associate Professor, Department of Mechanical Engineering, P.O. Box 11365-9587, Azadi Avenue; currently Aerospace Consultant, 11 Fox Run, Woodbury, Connecticut 06798. Senior Member AIAA.

†Associate Professor, Department of Mechanical Engineering, P.O. Box 11365-9587, Azadi Avenue; currently Associate Research Professor, Institute of Transportation Studies, University of California, Davis, One Shields Avenue, 2028 Academic Surge, Davis, California 95616. Member AIAA.

‡Ph.D. Candidate, Department of Mechanical Engineering, P.O. Box 11365-9587, Azadi Avenue.

low-, high-, and band-pass filters, a Pentium PC that allowed high sampling rate of data, appropriate software to manage and record the data, and a fast Fourier transform set of software to analyze the data in terms of frequency content and power spectrum. The high-frequency data channel were sampled at 200 kHz and filtered at 50 kHz. The signal-to-noise ratio for the data acquisition system was better than 100.

Motor Configuration

The motors that were designed to study the effects of grain geometry on combustion instability are depicted in Fig. 1. Excluding the nozzle section, all motors were 1193 mm long with an inside diameter of 101 mm giving them a final length-to-diameter ratio (L/D) of nearly 12. The actual initial L/D ratio based on grain configuration was nearly 37. These motors oscillated at a fundamental longitudinal frequency of approximately 425 Hz and were made in two equal segments, fitted with propellant cartridges cast in commercial off-the-shelf high-pressure PVC tubes. The forward face of each cartridge was inhibited using a 3-mm layer of commercial silicon sealant. This sealant burns into an ash-like composition, which is entirely washed away by the mean flow gas. The aft faces were allowed to burn. The nozzle section of tested motors had a throat diameter of 30 mm for the higher burning rate metalized propellant and 20 mm for the nonmetalized propellant. The forward section was designed to fit a centrally placed igniter, a ballistic pressure transducer (stain-gauge-type transducer), a high-frequency pressure transducer, and two pulsers.

Three basic grain configurations were employed in this study: a CP with 90% loading density, a short-armed seven pointed star (STAR) with 91% loading density and initial perimeter of 223 mm, and a long-armed seven pointed star (BOOST) with 86.5% loading density and initial perimeter of 353 mm (see Fig. 2). Four motors were produced from combination of these basic grains, each having a unique and completely different internal geometry. The grain geometries were CP forward-CP aft, CP forward-BOOST aft, STAR forward-STAR aft, and STAR forward-CP aft. Grain arrangements, in tested motors, are shown in Fig. 3. Of all possible grain arrangements the CP-CP, CP-STAR, STAR-STAR, and CP-BOOST grain configurations are of divergent port type. The CP-CP and STAR-STAR configurations are initially of constant-port-type grains. However, after motor ignition the erosive burning quickly renders these grains a divergent port configuration. The case of the CP-STAR, which is not a practical booster-sustainer configuration, was eliminated from consideration because we opted to test the limiting cases of CP-CP and CP-BOOST. We believed that if the limiting cases

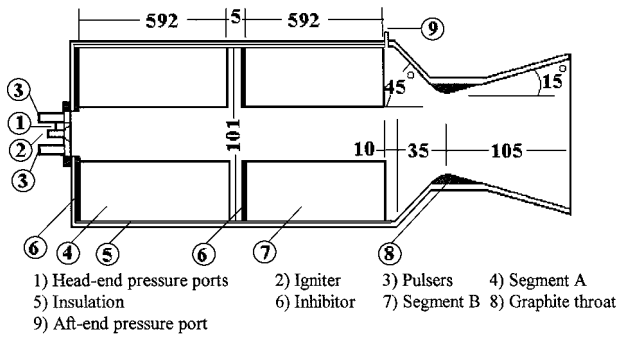

Fig. 1 Schematic of a pulsed tactical motor.

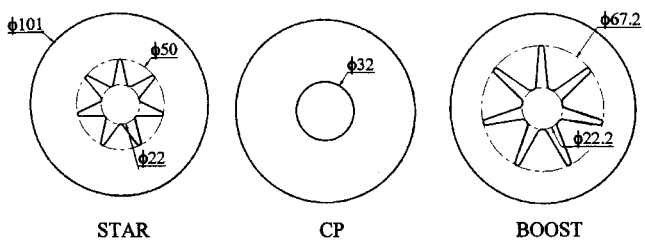

Fig. 2 Geometry of three basic grains.

Table 1 Solids content and size distributions

Ingredient	Class	Size, μ	Percent of total solids
AP	Fine	0–10	11.3
	Medium	106–125	35
	Coarse	355–425	53.7
Al	Fine	0–38	30
	Medium	38–53	20
	Coarse	53–90	50

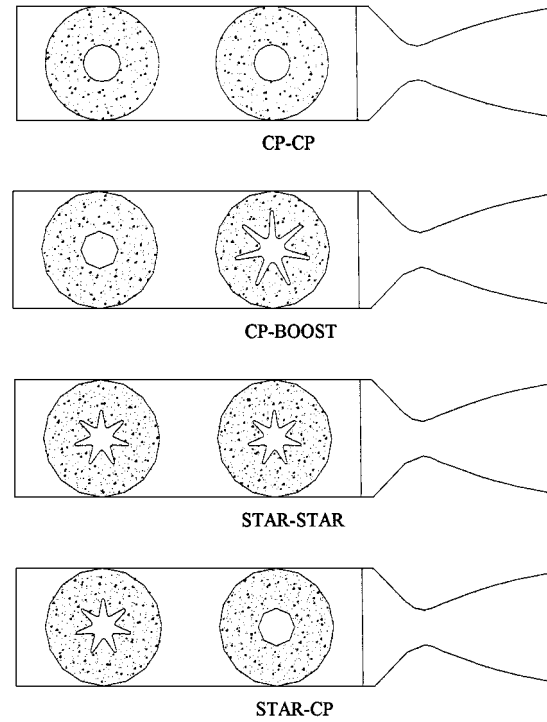

Fig. 3 Grain configurations in tested motors.

were shown to be linearly stable, then so would be the CP-STAR grain. In fact, in Ref. 11 it is shown that a CP-STAR configuration is indeed linearly stable and prone to instability, therefore proving our reason for omitting this test case.

Propellant Formulation

The basic propellant formulated for use in this investigation was a cast composite PU and AP containing 81% solids. No burn rate or stability additives were used in this formulation. The AP particle size distribution is given in Table 1. The initial formulation lacked any metal additive and was designated as propellant M5. Propellant M5 produced spontaneous pressure-coupled oscillations when tested in a variable area T-burner[15] at pressures and frequencies corresponding to that of the tested motors.

To eliminate the possible appearance of the high-frequency combustion oscillations, characteristic of nonmetalized solid propellants, the formulation was slightly varied; a small amount of oxidizer content was replaced with aluminum powder. This propellant (designated as propellant M6) had 74% AP and 7% Al with the appropriate size distribution of the Al given in Table 1. The majority of tests reported here were carried out using propellant M6. Combustion gases characteristics and pressure exponent for M5 and M6 propellants are given in Table 2. The burn rates were measured in a 5-in. ballistic evaluation motor.

Pulser Design and Performance

A pulsing technique employing black gunpowder charge was developed to initiate an unstable motor behavior. The hardware for this pulser is shown in Fig. 4. The level of pressure pulse produced by this device varied depending on the amount of black powder charge, motor operating pressure, and motor free volume. The powder charge

Table 2 Combustion gases characteristics[a]

Propellant	Flame temperature, K	R, j/kg-K	γ	a, mm/s	n
M5	2400	327.9	1.176	5.7	0.187
M6	3800	372.1	1.196	7.1	0.201

[a]In the expression $\dot{r} = a(p/p_{\text{ref}})^n$, p_{ref} is 6.9 Mpa.

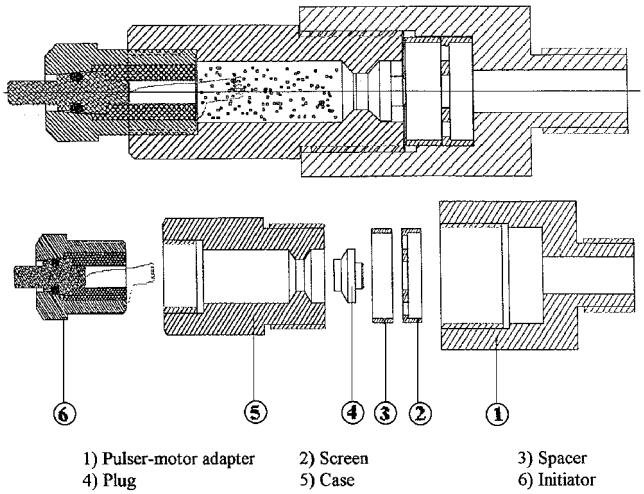

Fig. 4 Assembled pulser and its components.

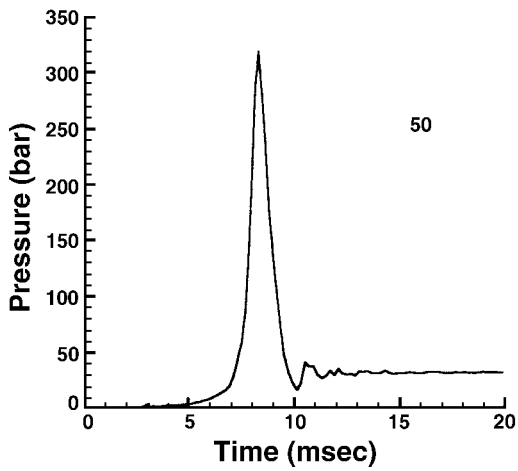

Fig. 5 Typical performance curve for a pulser.

used ranged from 300 to 500 mg depending on pulser initiation time. The pulser performance was analyzed using an accurate time-dependent one-dimensional gas dynamics code[16] and subsequently tested in steel tubes pressurized with nitrogen. The pressure vs time curve, measured for a typical pulser, is shown in Fig. 5.

On average, this pulsing device, which was installed on the head end of the motor, produced a pressure wave of about 10–15% of the mean motor pressure. These pulsers were very effective in initiating the axial mode instability in linearly stable motors. To ascertain the stability margin for the entire time of firing, a multiple pulsing technique was used in motors exhibiting stable behavior.

Test Methodology

As indicated in the Introduction, the goal of all subscale motors tested was to identify a suitable grain design for the full-scale tactical motor. The entire test matrix was comprised of 34 subscale motor firings. The main variable in all subscale tests was the internal grain geometry of the motor. To some very limited extent, propellant formulation and operating pressure were also investigated. Repeatability was investigated to confirm the observed behavior.

The test cases are described in Table 3, along with the overall stability status of fired motors: S for stable and U for unstable motor

Table 3 Selected test matrix for tested motors

Test ID	Number of pulses	P at Pulse, bar	DC shift, bar	Status
SSM5-1	0	——	——	S
SSM5-2	1	68	60	U
SSM6-1	0	——	——	S
SSM6-2	1	65	45	U
SSM6-3	1	85	35	U
CCM5-1	0	——	——	U
CCM5-2	1	40	100	U
CCM5-3	1	30	——	S
CCM6	1	70	80	U
CBM6-1	0	——	——	S
CBM6-2	1	62	40	U
CBM6-3	1	82	30	U
SCM5-1	0	——	——	S
SCM5-2	1	60	35	U
SCM5-3	1	62	36	U
SCM6-1	0	——	——	S
SCM6-2	1	75	——	S
SCM6-3	1	78	——	S
SCM6-4	2	75, 80	——	S

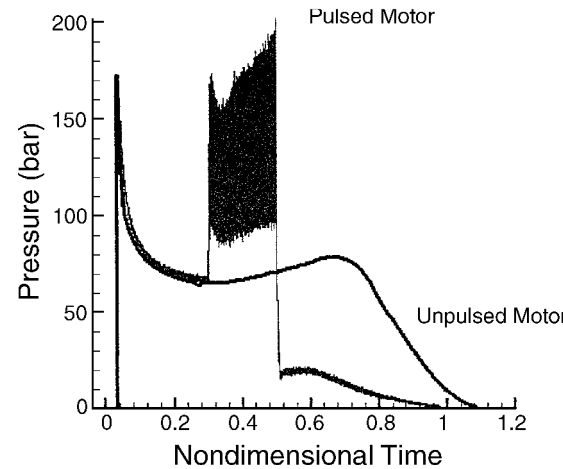

Fig. 6 Unstable performance of a pulsed motor identified as SSM5-2.

operation. The first two letters of test identification (ID) refers to the type of geometry. SS refers to a STAR-STAR, CC to a CP-CP, CB to a CP-BOOST, and SC to a STAR-CP grain configuration. The next two letters designate the propellant type, and numbers at the end signify the motor number for a given test case. At least one unpulsed motor firing was performed for a given test case. The pulsed motors were pulsed at the head end with up to two pulsers. These pulsers were designed to drive the motor unstable. An electronic timing device was used to control the pulser firing time. Two pressure transducers were used at the head end, and one fitted at the aft end just ahead of the nozzle entrance section.

Results and Discussion

Let us review what happens in an unstable tactical motor with a conventional solid propellant. In the case of a linearly unstable motor, low-amplitude pressure oscillations are spontaneously started and grow in time until eventually the magnitude of pressure oscillations reach the order of the motor's design pressure and result in its destruction. Nonlinear instabilities are caused by some external agent creating a momentarily increase in the pressure field. Nonlinear pressure fluctuations result in an appreciable dc shift in the motor's mean pressure level, which indicates a higher rate of energy release.

The head-end pressure vs time taken from a motor firing with a STAR-STAR grain configuration using propellant M5 is shown in Fig. 6. At nondimensional time of 0.28, a pulse is initiated, and nonlinear oscillations are triggered, leading to unstable behavior. In about 14 wave cycles the mean pressure changed from nearly 68 bar to about 120 bar.

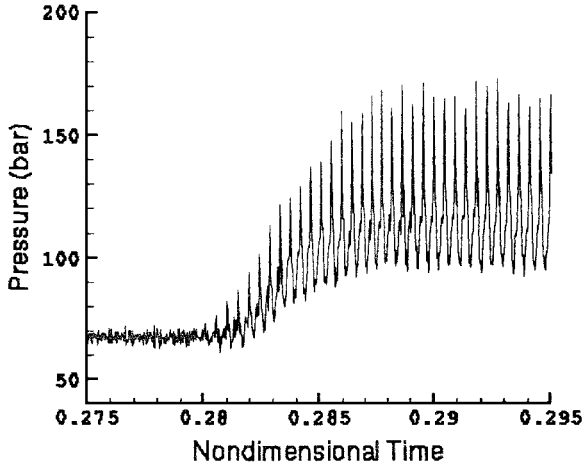

Fig. 7 Details of instability onset in SSM5-2 test.

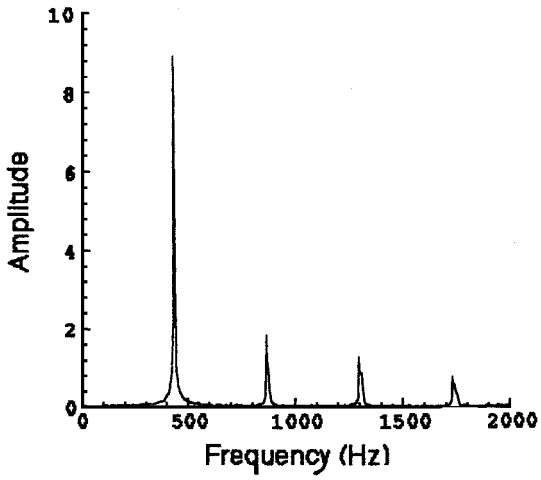

Fig. 8 Components of oscillatory pressure in frequency space of SSM5-2 test.

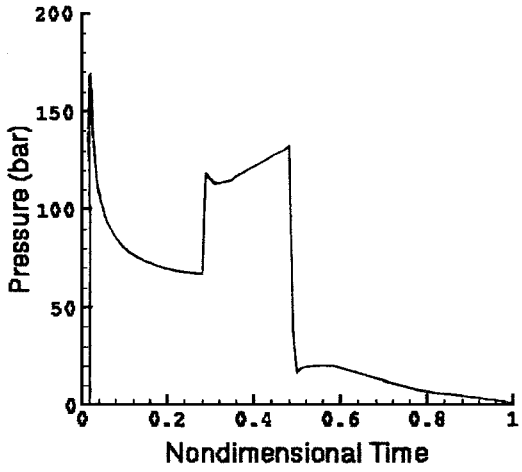

Fig. 9 Mean pressure of SSM5-2 test.

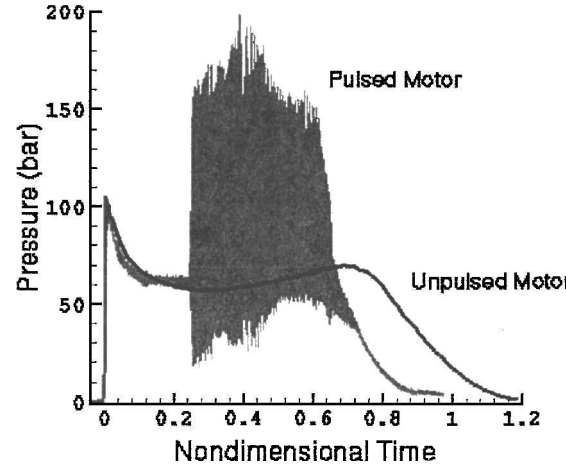

Fig. 10 Unstable performance of a pulsed motor designated as SSM6-2.

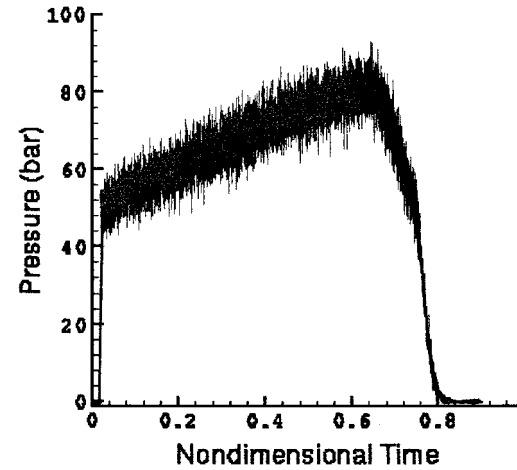

Fig. 11 Self-initiated linear unstable behavior of the motor designated as CCM5-1.

Details of instability onset are depicted in Fig. 7. Figure 8 shows the oscillatory pressure amplitudes in frequency space. As shown in this figure, a steep-fronted pressure wave with harmonic frequencies of 432, 864, 1298, and 1735 Hz develops during sustained instability. The first longitudinal mode dominates, with lesser contributions from other modes.

The mean motor pressure, without oscillatory components, is shown in Fig. 9. This pressure is seen to steadily increase with a finite, but constant rate. This increase could be caused by fast erosion of STAR geometry and gradual transformation to a mere CP geometry. A peak just like the initial erosive burning peak is also evident at nondimensional time of 0.3.

Finally, at nondimensional time of 0.48 the high level of pressure caused the graphite nozzle insert to shear and break away with a subsequent fall in the motor mean pressure. The pressure oscillation was abruptly damped and vanished as a result of this fast pressure decay.

To see the effect of metal aluminum powder on stability performance of the STAR-STAR grain, propellant M6 was used in the next test. The head-end pressure record for this test is shown in Fig. 10. As shown in this figure, once the pulser is triggered the motor goes into an unstable mode, with a dc shift of about 45 bar. Near burnout of the propellant, decay of pressure causes a gradual damping of oscillations. The amplitude of the pressure oscillation in this motor was more than twice that of the same motor tested with the nonmetalized propellant M5. Although the presence of condensed phase in the combustion products offer substantial damping, which manifests itself in relatively slow formation of the dc shift phenomenon, it is evident that the combustion of aluminum will also contribute to the level of energy available in the motor. In the case of nonlinear oscillations, this can result in larger amplitude pressure oscillations. The modes of oscillation for this test are the same as SSM5-2 test, with a small difference caused by higher speed of sound in the motor cavity caused by higher flame temperature.

The next series of tests focuses on the CP-CP grain geometry. The first motor tested in this series used the nonmetalized propellant M5. No pulser was planed for this test. However as shown in Fig. 11, right after the motor ignition a self-excited low-amplitude pressure

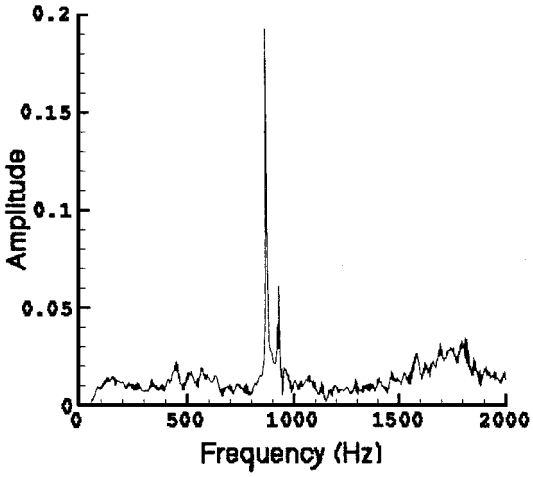

Fig. 12 Components of oscillatory pressure in frequency space of CCM5-1 test.

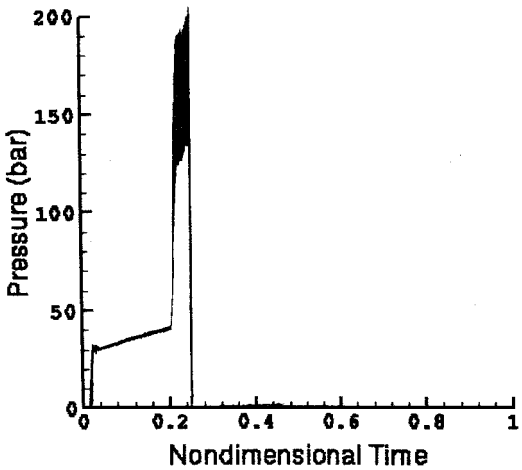

Fig. 13 Unstable performance of the motor labeled CCM5-2.

oscillation developed. The absence of a dc shift phenomena reveals that these fluctuations are of linear nature. The amplitude of oscillations remained constant during the entire motor firing. As can be seen from Fig. 12, the frequency of these oscillations corresponds to the second longitudinal mode of the motor chamber.

To see if the same pattern of instability was repeatable at different pressures, the nozzle throat diameter was increased from 20 to 22 mm. As depicted in Fig. 13, this resulted in reducing the initial pressure from 48 to nearly 30 bar. Although this change in pressure eliminated the initial pattern of self-excitation, initiation of a pulser at nondimensional time of 0.2 caused a dc shift of about 100 bar. The graphite throat insert was completely popped, and a dynamic extinction associated with fast changes in pressure (dp/dt extinction) occurred. Because of partial damage of high-frequency pressure transducer, complete data reconstruction was not possible. A low-frequency data analysis (using a 2-kHz low-pass filter) indicated that the first four modes of oscillations appeared right after the pulse.

The nozzle throat diameter was again increased from 22 to 24 mm, with a net reduction of the mean pressure from 30 to 22 bar. As can be seen from Fig. 14, a pulser of 10.2% strength was triggered at the nondimensional time of 0.2. The motor was unresponsive to this pulse and continued to burn stable. Consistent with other studies (see Refs. 10 and 12), it is evident that stability margin had increased with decreasing pressure. However, it is possible that greater pulse amplitude could have driven the motor unstable.

From a ballistic point of view, the case of the CP-CP grain configuration offers very little incentive. However, it can provide an excellent avenue for studying the pressure dependency of combustion

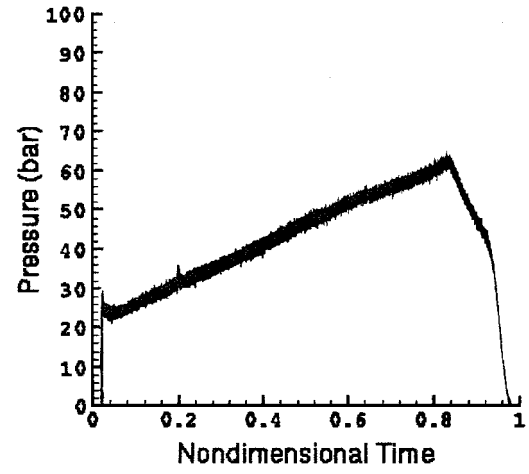

Fig. 14 Stable performance of a motor labeled CCM5-3.

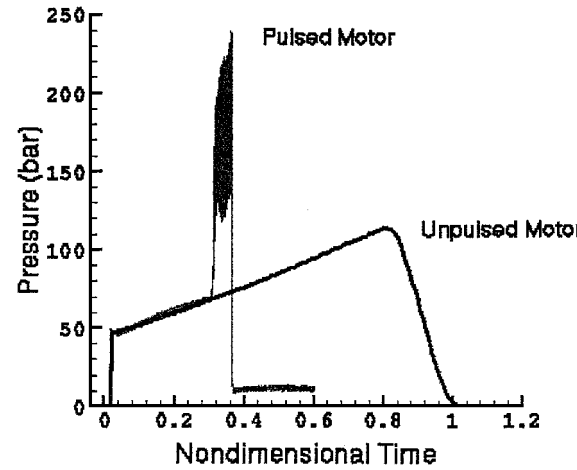

Fig. 15 Unstable performance of the motor labeled CCM6.

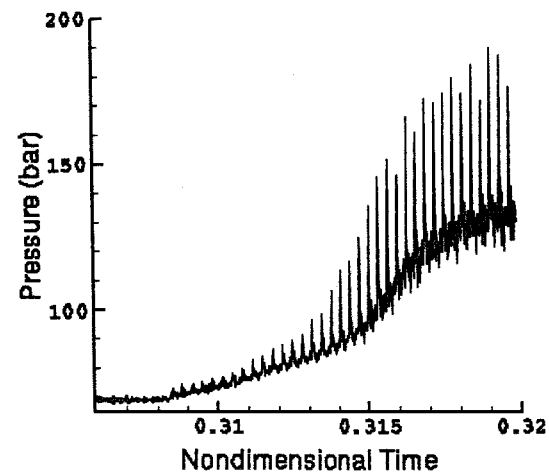

Fig. 16 Details of instability onset in CCM6 test.

instability. In any event more detailed experimental and theoretical analyses are warranted.

The same motor with a CP-CP grain behaves quite differently with metalized propellant M6. Figure 15 depicts the head-end pressure for this motor. A pulser is trigged at 0.30 nondimensional time during stable operation. Within 30 periods of oscillation, a dc shift had developed, which raised the pressure from 70 to about 150 bar. Mechanical failure of nozzle throat insert caused the mean pressure to drop to about 10 bar at 0.38 nondimensional time, and once again this rapid decrease of pressure causes oscillations to completely vanish. Details of instability onset are depicted in Fig. 16.

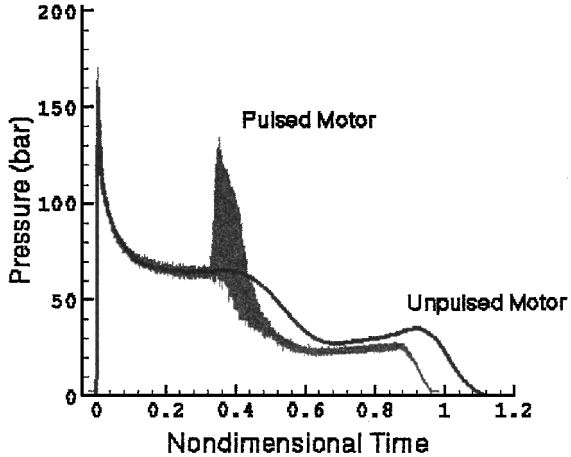

Fig. 17 Unstable performance of a pulsed motor designated as CBM6-2.

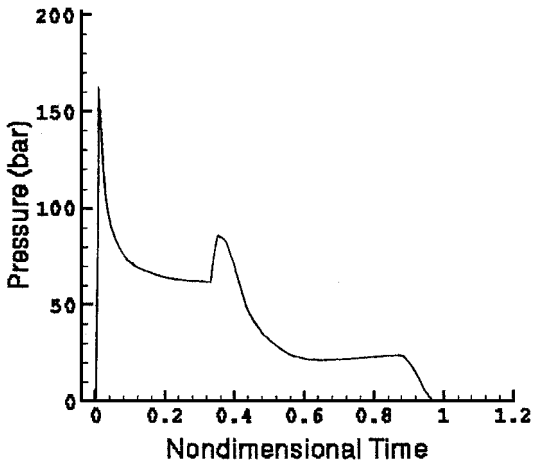

Fig. 18 Mean pressure deduced from CBM6-2 test.

In all tests reported so far, the internal geometry of the motor was uniform along the axis of the motor. To produce variable port area, motors were fitted with different grain cartridges. Combination of CP, STAR, or BOOST grains, as CP-BOOST and STAR-CP configurations, provided a variable gas port area through the length of the motor.

Motors with the CP-BOOST grain configuration show unstable behavior after pulse similar to the CP-CP and the STAR-STAR grain configurations. M5 and M6 propellants behave quite the same in this respect. Two sample tests, using M6 propellant, are discussed next. The head-end pressure record for the CP-BOOST case is shown in Fig. 17. Unstable oscillations, accompanied by a dc shift, are formed after a pulser is triggered at 0.35 nondimensional time. As the BOOST segment burns out, oscillations are shown to dampen, and the motor reverts to stable operation. Again, the effect of negative rate of the mean pressure change with time is worth noting. The mean pressure for this test is shown in Fig. 18. As indicated in this figure, after the formation of a dc shift the mean pressure starts to fall.

There is another interesting result associated with this test. In Fig. 19 pressure oscillation is shown in frequency space. Only the second and fourth modes are present, and odd modes are completely absent. Because the tested motor had equal length segments, it seems that theses modes could actually be associated with the first and second modes of the eroding BOOST segment.

In another test with the CP-BOOST grain, a pulse is employed shortly after the pressure starts to fall. This corresponds to the end of the boost phase of motor operation. The pressure versus time record for this test is shown in Fig. 20. In this test, similar to the last one, instability is started, and a dc shift is formed. After a short

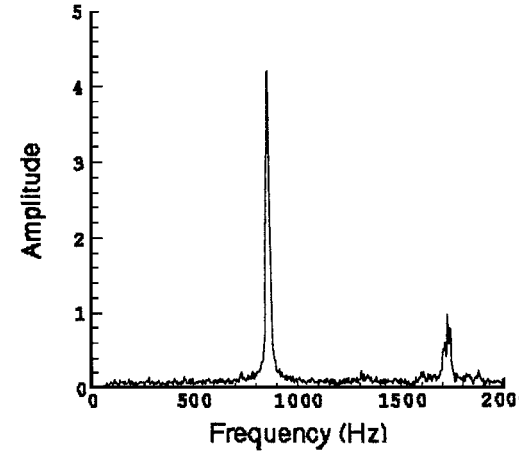

Fig. 19 Components of oscillatory pressure in frequency space of CBM6-2 test.

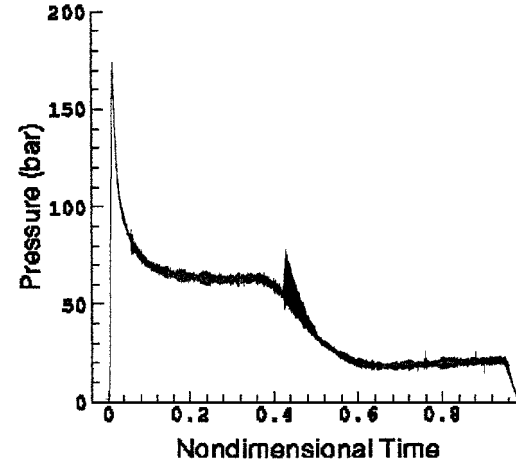

Fig. 20 Mean pressure of a pulsed motor designated as CBM6-3.

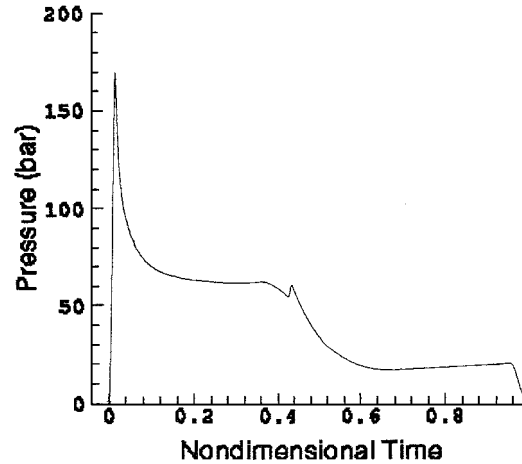

Fig. 21 Mean pressure of CBM6-3 test.

period instability is damped, and the motor shows stable behavior for the remainder of its burning time. The nature of this behavior is similar to the last test. Close examination of the mean pressure taken from this test, shown in Fig. 21, indicates a much smaller dc shift. Components of oscillatory waves in frequency space are shown in Fig. 22. Second, third, and fourth modes of oscillations are present, whereas the first mode is completely absent. This result is in sharp contrast to the preceding one.

Despite the geometric differences between STAR-STAR, CP-CP, and CP-BOOST grain configurations, patterns of combustion

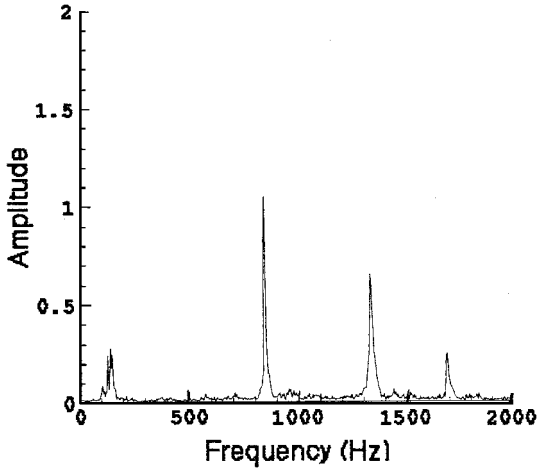

Fig. 22 Components of oscillatory pressure in frequency space of CBM6-3 test.

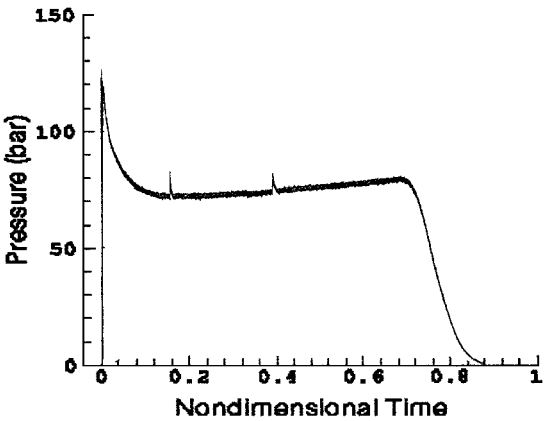

Fig. 23 Stable performance of a double-pulsed motor designated as SCM6-4.

instability occurring in them are similar. Examination of grain burnback patterns reveals a constant or a divergent port area through motor operation. In other words, in all cases studied so far the mean pressure has a progressive change, and its rate is positive in terms of time and space.

This brings us to the case of STAR-CP grain configuration. Two motors were tested with this configuration using M6-type propellant. They both showed stable behavior after single pulses were applied. The only difference between the two was the pulser initiation times. As a result, a two-pulse test was planned for this motor. Pressure records are shown in Fig. 23. The pulses were applied at 0.18 and 0.4 nondimensional times. The strengths of the pulses were 14.6 and 11.9%, respectively. Despite multipulse application, this configuration offered great stability margin during entire motor firing.

Recent results obtained by Elhami-Amiri[17] strengthen our belief that in any fluid system, especially in a solid rocket motor, the balance between available energy for fluid acceleration or deceleration and wave propagation is the key to an overall stability or instability. In other words, if fluid particles are globally and uniformly accelerating very little energy is available for wave propagation, and this condition is not favorable to instability; whereas the reverse is true for the case of deceleration. In uniform gas port area, such as the STAR-STAR or the CP-CP grain configuration, erosive effects causes a widening of port area from head end to aft end, decreasing gas velocity and therefore a condition suitable for instability. The same is true about the CP-BOOST case. In contrast, the STAR-CP grain offers a closure of port area. This closure increases the gas velocity and provides a favorable stability condition.

Conclusions

The effects of grain geometry on combustion instability of tactical solid-propellant rocket motors were studied in this paper. Although the conclusions of this study were highlighted throughout the paper, they will be reiterated here for future reference.

Among the four grain configurations studied, the case of STAR-CP is the most stable, especially when used with a metalized propellant. This grain design has been successfully implemented in a full-scale motor; repeated testing of which has shown an excellent envelop of combustion stability. Our study confirms the results of Ref. 14 that grain geometries offering a closure of port area will provide a favorable stability condition, whereas the reverse is true for grains with divergent port area. As noted by one of the reviewers of this paper, because our grains as well as the ones used in Refs. 11 and 14 had rather abrupt area changes a series of tests could be performed using simple convergent and divergent conical grains.

Casting of such grains in an operational motor does pose some new challenges. However, the benefit offered in terms of combustion instability damping far outweighs the manufacturing problems that need to be overcome.

Based on the observations made in this study, further experimental and analytical investigations are required to answer the following key questions:

1) What are the mechanisms of wave energy transfer between various frequencies in an unstable solid-propellant rocket motor?

2) What is the role of high negative dp/dt during any phase of the motor operation in preventing the occurrence of combustion instability?

3) How does coupling between the kinetic energy of mean flow and the energy needed for sustained oscillations affect the overall stability of a motor?

It is our belief that our limited amount of testing and the lack of any analytical analysis have added more questions than answering the existing ones, but it is hoped that the test data, discussions, and questions raised herein will add to our overall understanding of combustion instability.

Acknowledgments

The authors wish to thank the Jahad Engineering and Research Center for their technical and financial support. The authors would also like to thank the Research Office of the Sharif University of Technology for providing partial financial funding of this project. Numerous graduate students from the Sharif University of Technology collaborated on this research; their endeavors are greatly appreciated.

References

[1] Karnesky, A. L., and Colucci, S. E., "Recent Occurrences of Combustion Instability in Solid Rocket Motors—An Overview," *Journal of Spacecraft and Rockets*, Vol. 12, No. 1, 1975, pp. 33–38.

[2] Price, E. W., "Combustion Instability in Solid Rocket Motors: Executive Summary," Chemical Propulsion Information Agency, CPIA Pub. 290, Vol. I, Laurel, MD, Nov. 1977.

[3] Price, E. W., "Experimental Observation of Combustion Instability," Chapter 13, *Fundamentals of Solid-Propellant Combustion*, edited by K. K. Kuo and M. Summerfield, AIAA, New York, 1984, Chap. 13, pp. 733–790.

[4] Flandro, G. A., "Vortex Driving Mechanism in Oscillatory Rocket Flows," *Journal of Propulsion and Power*, Vol. 2, No. 3, 1986, pp. 206–214.

[5] Vuillot, F., "Vortex Shedding Phenomena in Solid Rocket Motors," *Journal of Propulsion and Power*, Vol. 11, No. 4, 1995, pp. 626–639.

[6] Kourta, A., "Acoustic-Mean Flow Interaction and Vortex Shedding in Solid Rocket Motors," *International Journal of Numerical Methods in Fluids*, Vol. 22, No. 6, 1996, pp. 449–465.

[7] Dotson, K. W., Koshigoe, S., and Pace, K. K., "Vortex Shedding in a Large Solid Rocket Motor without Inhibitors at the Segment Interfaces," *Journal of Propulsion and Power*, Vol. 13, No. 2, 1997, pp. 197–206.

[8] Hart, R. W., and McClure, F. T., "Theory of Acoustic Instability in Solid Propellant Combustion," *Proceedings of the Tenth International Symposium on Combustion*, The Combustion Inst., Pittsburgh, PA, 1965, pp. 1047–1065.

[9]T'ien, J. S., "Theoretical Analysis of Combustion Instability," *Fundamentals of Solid-Propellant Combustion*, edited by K. K. Kuo and M. Summerfield, AIAA, New York, 1984, Chap. 14, pp. 791–840.

[10]Brownlee, W. G., "Nonlinear Axial Combustion Instability in Solid Propellant Motors," *AIAA Journal*, Vol. 2, No. 2, 1964, pp. 275–284.

[11]Blomshield, F. S., Crump, J. E., Mathes, H. B., Stalnaker, R. A., and Beckstead, M. W., "Stability Testing of Full-Scale Tactical Motors," *Journal of Propulsion and Power*, Vol. 13, No. 3, 1997, pp. 349–355.

[12]Blomshield, F. S., Mathes, H. B., Crump, J. E., Beiter, C. A., and Beckstead, M. W., "Nonlinear Stability Testing of Full-Scale Tactical Motors," *Journal of Propulsion and Power*, Vol. 13, No. 3, 1997, pp. 356–366.

[13]Harris, P. G., and De Champlain, A., "Experimental Database Describing Pulse-Triggered Nonlinear Instability in Solid Rocket Motors," *Journal of Propulsion and Power*, Vol. 14, No. 4, 1998, pp. 429–439.

[14]Koreki, T., Aoki, I., Shirota, K., and Toda, Y., "Experimental Study on Oscillatory Combustion in Solid-Propellant Motors," *Journal of Spacecraft and Rockets*, Vol. 13, No. 9, 1976, pp. 534–539.

[15]Farshchi, M., Golafshani, M., Ghassemi, H., Mohamed, K., and Javadi, J., "T-burner Studies of the M5 and M6 Solid Propellants," Jahad Engineering and Research, Rept. No. JERC-1377, Tehran, Iran, Feb. 1999.

[16]Saleh, M. K., "One Dimensional Transient Solution of Gas-Particle Flow in a Solid Rocket Motor," M.S. Thesis, Dept. of Mechanical Engineering, Sharif Univ. of Technology, Tehran, Iran, Sept. 1998.

[17]Elhami-Amiri, A., "The Development of an Accurate Time Dependent, Three-Dimensional Flow Solver to Study the Effects of Geometry on Acoustic Instability in SRMs," M.S. Thesis, Dept. of Mechanical Engineering, Sharif Univ. of Technology, Tehran, Iran, Sept. 1999.